JOURNAL OF AIRCRAFT
Vol. 41, No. 1, January–February 2004

Minimum-Induced Power Loss of a Helicopter Rotor via Circulation Optimization

Omri Rand* and Vladimir Khromov†
Technion—Israel Institute of Technology, 32000 Haifa, Israel
and
Richard J. Peyran‡
U.S. Army Aviation and Missile Command, NASA Ames Research Center, Moffett Field, California 94035

The paper summarizes a study aimed towards determining the lower limit of induced power of helicopter rotors in hover and forward flight. The current optimization study was not based on design parameters such as rotor-blade chord, airfoil, and twist angle distributions. Instead, the rotor-disc bound circulation radial and azimuthal distributions were selected to be the independent unknowns in the minimization process of the induced power. Hence, the optimization results set the lower realistic bound of rotor-induced power. The results can serve as a useful reference for designers evaluating current and future rotor system performance.

Nomenclature

c	=	blade chord
c_D	=	sectional drag coefficient
c_L	=	sectional lift coefficient
c_{M_X}	=	rotor pitch-moment coefficient
c_{M_Y}	=	rotor roll-moment coefficient
c_T	=	rotor thrust coefficient
c_P	=	rotor induced power coefficient
F_{ij}^{l}	=	far-wake influence coefficient
K_F	=	number of harmonics
M_X	=	rotor pitch moment
M_Y	=	rotor roll moment
N_{ij}^{kl}	=	near-wake influence coefficients
N_R	=	number of spanwise segments
N_ψ	=	number of azimuthal sectors
P	=	rotor-induced power
R	=	rotor radius
T	=	rotor thrust
U	=	sectional freestream velocity
$v(r, \psi)$	=	induced velocity
α	=	angle of attack
$\Gamma(r, \psi)$	=	bound vortex circulation
Θ_{twist}	=	linear twist rate
Θ_0	=	collective pitch angle
μ	=	advance ratio
ρ	=	air density
σ	=	rotor solidity
ψ	=	azimuth angle
Ω	=	rotor rotational speed

Introduction

THE induced power is a major component of the power required in helicopters and is of the order of 70% of the total power required in hover and has a significant influence in forward flight as well. Thus, any reduction of this component can lead to a considerable performance improvement. The induced power is a strong function of the bound circulation distribution over the disc, and therefore, the optimization of this distribution is the focus of the present paper.

The phenomena related to the induced power of a helicopter rotor involve some classic analysis, most of which is well documented in various textbooks (i.e., Refs. 1 and 2). A review of the associated physics is beyond the scope of the present paper. The problem of minimum induced power has been directly addressed in Refs. 3–5 and indirectly in many studies of higher harmonic control where a reduction in the power required has been obtained for various modes of this method (e.g., see Refs. 6 and 7).

In hover, by ignoring tip effects and nonlinear wake effects, one can show that uniform disc loading (i.e., uniform circulation distribution) results in a uniform induced velocity distribution and minimum induced power. In forward flight the product of the mean induced velocity and the rotor thrust are commonly used as the "ideal" induced power consumption. However, because of the complexity of the flowfield in the rotor vicinity it is not clear that the induced power levels obtained by the assumption of uniform induced velocity and loading are valid as ideal reference values. In addition, from a design point of view it is interesting to explore the lower realistic limit of the induced power and to evaluate the gap between a specific blade design and the most efficient rotor.

Proposed Methodology

To estimate the minimum induced power of a helicopter rotor in hover and forward flight, it is suggested to consider the radial and azimuthal distributions of the bound vortices as the independent unknowns in an optimization process. Such a procedure leaves design parameters such as chord, airfoil, and twist angle distributions out of the optimization loop and, therefore, provides a generic, achievable, minimum value for the induced power. As will be shown later on, in forward flight this minimal value might not always be easily realized by conventional design parameters because it requires a circulation distribution that might not be implemented through constant distributions of blade chord, twist, airfoil, and cyclic pitch controls.

To formulate the proposed optimization procedure, we will denote the bound vortex distribution $\Gamma(r, \psi)$ and the induced power P. The proposed optimization scheme can be therefore expressed as

$$\text{Minimize} \qquad P \qquad \text{Over} \qquad \Gamma(r, \psi) \tag{1}$$

subjected to the constraints:

$$g_n = \frac{1}{2\pi} \int_0^{2\pi} \int_0^R \Gamma(r, \psi) f_n(r, \psi)\, \mathrm{d}r\, \mathrm{d}\psi, \qquad n = 1, N_C \tag{2}$$

Received 6 June 2002; revision received 29 April 2003; accepted for publication 29 April 2003.

*Professor, Faculty of Aerospace Engineering. Member AIAA.
†Researcher, Faculty of Aerospace Engineering.
‡Aerospace Engineer, Aeroflightdynamics Directorate, Advanced Design Team.

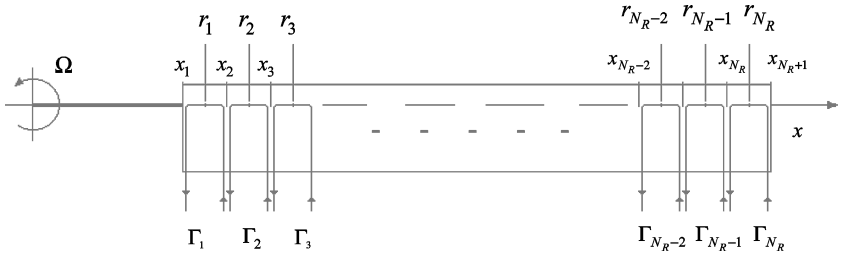

Fig. 1 Blade radial discretization.

where g_n and $f_n(r, \psi)$ are given sets of scalars and functions, respectively.

To facilitate the derivation, the sectional lift is expressed using a single bound vortex at the quarter-chord location (see Fig. 1 for a scheme of the blade radial discretization). Thus, the lift per unit length is given by:

$$\frac{\mathrm{d}L}{\mathrm{d}r}(r, \psi) = \rho U(r, \psi)\Gamma(r, \psi) \tag{3}$$

Referring to a Cartesian system of coordinates where Y is directed backwards (i.e., opposite to the flight direction) and Z is directed downwards, the rotor thrust, pitching moment, rolling moment, and induced power are given by

$$[T, M_X, M_Y, P] = \frac{N_B}{2\pi}\int_0^{2\pi}\int_0^R \frac{\mathrm{d}L}{\mathrm{d}r}[1, -r\cos\psi, r\sin\psi, v]\,\mathrm{d}r\,\mathrm{d}\psi \tag{4}$$

Note that flapping and any other motion of the blade need not be considered here because as already stated, we are looking for the optimal circulation distribution only. Subsequently, the source of this distribution is immaterial as it can emerge from blade motion, active devices, etc.

The disc is discretized into N_ψ azimuthal sectors, whereas the blade is discretized into N_R spanwise segments. Subsequently, the nondimensional thrust, moments, and power per blade can be expressed in the following nondimensional and discrete manner:

$$\frac{c_T}{\sigma} = \frac{1}{2\pi}\frac{R}{\bar{c}}\sum_{j=1}^{N_\psi}\sum_{i=1}^{N_R} G(\tilde{r}_i, \psi_j) \tag{5a}$$

$$\frac{c_{Mx}}{\sigma} = \frac{1}{2\pi}\frac{R}{\bar{c}}\sum_{j=1}^{N_\psi}\sum_{i=1}^{N_R} -\tilde{r}_i\cos\psi_j G(\tilde{r}_i, \psi_j) \tag{5b}$$

$$\frac{c_{My}}{\sigma} = \frac{1}{2\pi}\frac{R}{\bar{c}}\sum_{j=1}^{N_\psi}\sum_{i=1}^{N_R} \tilde{r}_i\sin\psi_j G(\tilde{r}_i, \psi_j) \tag{5c}$$

$$\frac{c_P}{\sigma} = \frac{1}{2\pi}\frac{R}{\bar{c}}\sum_{j=1}^{N_\psi}\sum_{i=1}^{N_R} \tilde{v}(\tilde{r}_i, \psi_j) G(\tilde{r}_i, \psi_j) \tag{5d}$$

where

$$G(\tilde{r}_i, \psi_j) = (\tilde{r}_i + \mu\sin\psi_j)\tilde{\Gamma}(\tilde{r}_i, \psi_j)\Delta\tilde{r}\Delta\psi \tag{6}$$

and σ based on the the averaged chord $\bar{c}$, $\tilde{v} = v/(\Omega R)$, $\tilde{\Gamma} = \Gamma/(\Omega R^2)$, and $\tilde{r} = r/R$. Note that $\bar{c}$ appears just for the sake of introducing σ into the formulation as it is immaterial in the present optimization process.

Based on the preceding discretization, the independent unknowns are the $N_\psi \times N_R$ bound vortices strengths. To reduce the number of the problem independent unknowns, a Fourier-series representation of the bound circulation in the azimuthal direction was adopted. Using a standard Fourier-series expansion, the circulation at $r = r_i$ and $\psi = \psi_j$ can be written as

$$\tilde{\Gamma}(i, j) \cong \tilde{\Gamma}_0(i) + \sum_{k=1}^{K_F}[\tilde{\Gamma}_s(i, k)\sin k\psi_j + \tilde{\Gamma}_c(i, k)\cos k\psi_j] \tag{7}$$

Substituting Eq. (7) in Eqs. (5a–5c) and carrying out the integrations with respect to ψ (analytically) yields

$$\frac{c_T}{\sigma} = \frac{R}{\bar{c}}\sum_{i=1}^{N_R}\frac{1}{2}[2\tilde{r}_i\tilde{\Gamma}_0(i) + \mu\tilde{\Gamma}_s(i, 1)]\Delta\tilde{r} \tag{8}$$

$$\frac{c_{M_X}}{\sigma} = -\frac{R}{\bar{c}}\sum_{i=1}^{N_R}\frac{\tilde{r}_i}{4}[2\tilde{r}_i\tilde{\Gamma}_c(i, 1) + \mu\tilde{\Gamma}_s(i, 2)]\Delta\tilde{r} \tag{9}$$

$$\frac{c_{M_Y}}{\sigma} = \frac{R}{\bar{c}}\sum_{i=1}^{N_R}\frac{\tilde{r}_i}{4}[2\mu\tilde{\Gamma}_0(i) + 2\tilde{r}_i\tilde{\Gamma}_s(i, 1) - \mu\tilde{\Gamma}_c(i, 2)]\Delta\tilde{r} \tag{10}$$

Using this discretization form, the optimization should be carried out for $(2K_F + 1) \times N_R$ independent unknowns. This number is usually smaller than the one required when Fourier-series expansion is not used because the number of practical harmonics is usually not very high.

Wake Models and Influence Coefficients

The relatively low coupling between the wake geometry and the wake strength enables one to define and utilize the concept of wake-influence coefficients during the optimization process. This working mode substantially contributes to the efficiency of the optimization.

To implement the present optimization approach, two types of wake models were utilized. First, the lifting-line blade model combined with a prescribed wake model of RAPID (Rotorcraft Analysis for Preliminary Design; see Ref. 8) was used for initial study and process validation. Then, a free-wake geometry model from CAMRAD II (Comprehensive Analytical Model of Rotorcraft Aerodynamics and Dynamics; see Ref. 9) was introduced.

Within the rigid-wake model the blade is represented by a system of "horseshoe" vortices, each of which consists of a bound segment at the blade quarter-chord and two trailing branches. The wake model consists of two main components that emerge from each blade: an inboard trailing system and a tip trailing vortex. The system of inboard trailing vortices is (helically) stretched from each blade up to a prescribed wake age. From that age and on a tip vortex is (helically) stretched up to infinity while its strength is assumed to be the maximal bound vortex strength at the each azimuthal location. A core model is also utilized. For this model the inboard system is denoted as the near wake, and the tip vortex is denoted as the far wake.

The free-wake model used from CAMRAD II is described in Ref. 9. This model was developed to give good performance results both in hover and forward flight (Ref. 10). A free-wake geometry model offers advantages over a rigid-wake geometry model in hover and low-speed forward flight for predicting rotor performance and blade loading. Analyses have shown that a rigid-wake geometry model is less accurate at advance ratios below 0.15 (Ref. 10). When the rotor is in an operating condition such that the wake remains close to the disc, then the self-induced distortion of the wake geometry affects the loading, and a free-wake calculation is important. A single-peak bound circulation distribution was assumed. This is appropriate for advance ratios of 0.25 and below where the lift on the advancing side of the rotor disk is positive. (The current study was limited to advance ratios of 0.25 and below.)

The RAPID and CAMRAD II wake models provided the near-wake and far-wake influence coefficients required for the optimization process. These influence coefficients are used to calculate the rotor-induced velocity distribution and power as discussed in the next section.

The influence coefficients are defined by their role in the determination of the induced velocity:

$$v_{(i,j)} = \sum_{k=1}^{N_R} \sum_{l=1}^{N_\psi} N_{ij}^{kl} \Gamma_{(i,j)} + \sum_{l=1}^{N_\psi} F_{ij}^{l} \Gamma_{(l)}^{MAX} \tag{11}$$

where $\Gamma_{(i,j)}$ is the circulation intensity at $r = r_i$ and $\psi = \psi_j$ and $\Gamma_{(l)}^{MAX}$ are the radially maximal circulation intensities along the span at $\psi = \psi_l$ that determines the tip vortex intensity. In addition, N_{ij}^{kl} are the influence coefficients of the near wake, or, in other words, the velocity that is induced at $r = r_i$ on blade 1 when it is positioned at $\psi = \psi_j$ by all horseshoe vortices, which have been originated from $r = r_k$ and $\psi = \psi_l$ of all blades (i.e., blades $1, 2, \ldots, N_B$) while having a unit strength. Similarly F_{ij}^{l} are the influence coefficients that together with the magnitude of the maximal (radial) circulation distribution determine the velocity, which is induced by the far wake. For the free-wake model these definitions represent a single-peak circulation distribution model.

Cost Function

The cost function can be defined in various ways where different weighting values are assigned to the induced power and the aerodynamic moments on the rotor. In the present study the requirement that the rotor produces a given amount of thrust and zero aerodynamic moments on the rotor has been implemented. Thus, the cost function becomes

$$J = \frac{c_P}{\sigma} \tag{12}$$

To ensure that c_T/σ remains constant and that c_{M_X}/σ and c_{M_Y}/σ are zero for each trail vector of the optimizer, the optimization independent variables are the circulation harmonics $\tilde{\Gamma}_0(i)$, $\tilde{\Gamma}_s(i,k)$, and $\tilde{\Gamma}_c(i,k)$ for $i = 1, N_R$, $k = 1, K_F$, except for $\tilde{\Gamma}_0(i_0)$, $\tilde{\Gamma}_s(i_0, 1)$, and $\tilde{\Gamma}_c(i_0, 1)$. These values are obtained from Eqs. (8–10), where $\tilde{\Gamma}_0(i_0)$ and $\tilde{\Gamma}_s(i_0, 1)$ are obtained by solving Eqs. (8) and (10) simultaneously and $\tilde{\Gamma}_c(i_0, 1)$ is then obtained from Eq. (9). The station $\tilde{r}_{i_0}$ is typically selected as the closest location to 0.75. The total number of independent unknowns in this case (which is valid only for $K_F > 0$) is $(2K_F + 1)N_R - 3$.

Optimization Process

The optimization process is shown in Figs. 2 and 3. Figure 2 presents the outer loop, which is responsible for the iterations of the maximal circulation distribution, whereas the inner optimization loop is performed for constant maximal circulation values.

For a given maximal circulation distribution the optimization is based on a solution of a system of nonlinear equations, which generally can be expressed as

$$f_i(x_1, x_2, x_3, \ldots, x_M) = 0, \qquad i = 1, \ldots, M \tag{13}$$

where x_i is a $(2K_F + 1)N_R - 3$ length vector that contains the circulation coefficients, namely,

$$x_i = \left\langle \Gamma_0^1, \Gamma_0^2, \ldots, \Gamma_0^{N_R}, \Gamma_{s1}^1, \ldots, \Gamma_{s1}^{N_R}, \ldots, \Gamma_{s2}^{N_R}, \right.$$
$$\left. \ldots, \Gamma_{sN_\varphi}^{N_R}, \Gamma_{c1}^1, \ldots, \Gamma_{c1}^{N_R}, \ldots, \Gamma_{c2}^{N_R}, \ldots, \Gamma_{cN_\varphi}^{N_R} \right\rangle \tag{14}$$

As already indicated, $\tilde{\Gamma}_0(i_0)$, $\tilde{\Gamma}_s(i_0, 1)$, and $\tilde{\Gamma}_c(i_0, 1)$ are omitted. To ensure a minimal cost function, f_i are selected as the partial derivatives of the cost function with respect to the independent unknowns:

$$f_i = \frac{\partial J}{\partial x_i}, \qquad i = 1, \ldots, M \tag{15}$$

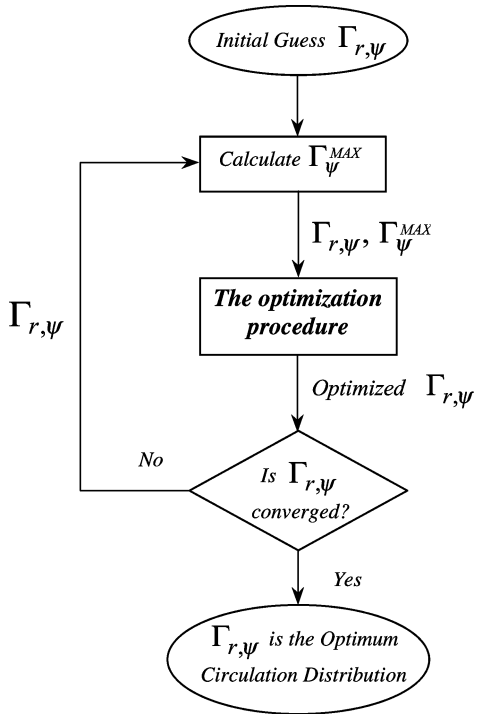

Fig. 2 Outer loop, which updates the maximal circulation values for the optimization procedure.

The preceding derivative is evaluated numerically. The overall numerical procedure is described in Fig. 3. As shown, for a trial vector x_i^0, a Jacobian matrix that contains all functions' sensitivity derivatives at the working point ($x_i = x_i^0$) is determined. This matrix is used in the following equation, which equates the correction vector $\hat{x}_i$ that is required to cancel out the residual $f_i(x_i^0)$ under the assumption of linear behavior of the functions f_i around the working point (quasi-linear assumption):

$$\begin{bmatrix} \frac{\partial f_1}{\partial x_1} & \cdots & \frac{\partial f_1}{\partial x_M} \\ \vdots & & \vdots \\ \frac{\partial f_M}{\partial x_1} & \cdots & \frac{\partial f_M}{\partial x_M} \end{bmatrix} \{\hat{x}_i\} = \begin{Bmatrix} -f_1(x_i^0) \\ \vdots \\ -f_M(x_i^0) \end{Bmatrix} \tag{16}$$

The preceding equation yields the correction vector $\hat{x}_i$, and unless $\hat{x}_i$ is sufficiently small it is added to x_i^0, and the preceding process is repeated until convergence is achieved.

As shown in Fig. 3, to determine the cost function the following steps are carried out. First, $\tilde{\Gamma}_0(i_0)$, $\tilde{\Gamma}_s(i_0, 1)$, and $\tilde{\Gamma}_c(i_0, 1)$ are calculated to ensure constant c_T and zero aerodynamic moments on the rotor. Then, the distribution $\tilde{\Gamma}(i, j)$ is determined [Eq. (7)], and the influence coefficients are used to determine the induced velocity. The induced velocity is then used to calculate c_P, and J [Eqs. (5d) and (12)]. To derive numerically the value of $\partial J/\partial x_i$ [see Eq. (15)], two subsequent calls for this procedure are required.

During the preceding described procedure, updating the wake geometry according to the current $\tilde{\Gamma}(i, j)$ (which leads to an updating of the influence coefficients) does not have to take place at each iteration. The present study has shown that updating the influence coefficients for free-wake analysis can take place only every 5–10 optimization steps.

To track the convergence path of the present analysis, an error between two successive iterations n and $n + 1$ was defined as

$$e = Max\left(\left| \frac{\Gamma_{ij}^{n+1} - \Gamma_{ij}^{n}}{\Gamma_{\text{Average}}^{n+1}} \right| \right) \times 100\% \tag{17}$$

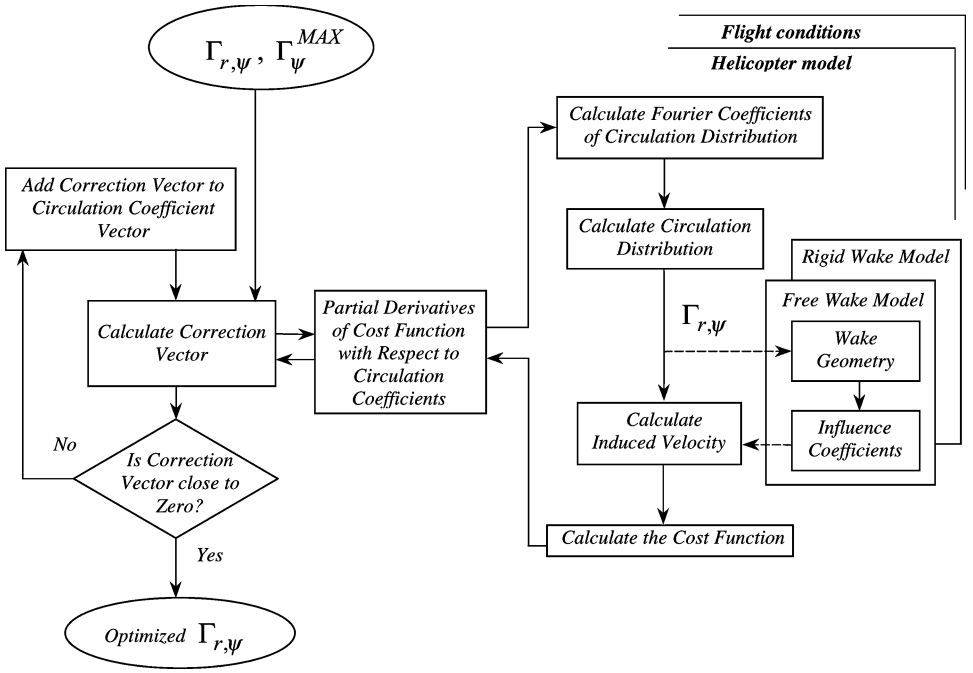

Fig. 3 Optimization procedure loop for constant maximal circulation values.

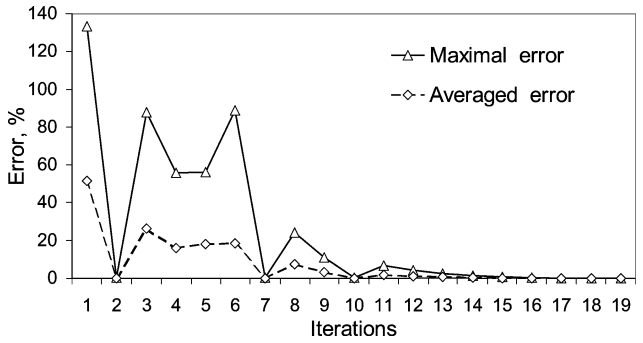

Fig. 4 Maximal and average error in circulation vs iterations for $\mu = 0.05$.

Fig. 5 Induced power coefficient vs iterations for $\mu = 0.05$.

Illustrative Results

The results presented here are for a four bladed 13.42-m-diam rotor. The blade-root cutout is $0.3R$, and the angular velocity is 30.7 rad/s. The shaft angle is set to zero in all cases. The rotor produces a thrust of $C_T = 0.0088$.

Figure 4 presents the maximal average and errors in circulation for $\mu = 0.05$. As shown, the error rapidly converges and practically vanishes for more than nine iterations. The convergence path of the power coefficient is presented in Fig. 5. It is shown that as a global characteristic the value of the minimum induced power converges even faster.

The rotor-induced power as a function of the forward flight velocity is presented in Fig. 6. The theoretical values that have been determined as the product of the thrust and the average (Glauert's model) induced velocity are shown as ideal values.

Also, the induced power of a reference rotor as calculated by CAMRAD II using a free-wake geometry analysis (without circulation optimization) is plotted. These values were obtained for a rotor of the same diameter that produces the same thrust and was trimmed to zero aerodynamic moments on the rotor and zero-tip-path-plane angle of attack. The twist and chord distribution of the reference rotor blades are shown in Figs. 7 and 8. This reference rotor represents a late-1970s advanced technology rotor. The reference rotor-blade geometry and airfoil distribution are described in Ref. 11. The root cutout was increased to $0.30R$ (from $0.14R$) to be consistent with the optimized rotor root cutout.

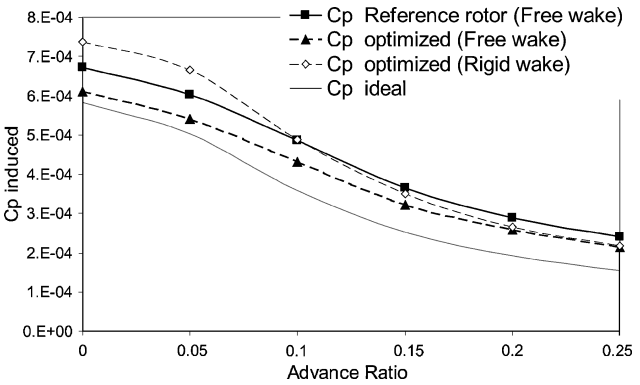

Fig. 6 Induced power coefficient vs advance ratio.

The optimized values obtained by the present analysis are shown to be located between the preceding two reference lines. It is also shown that practically the lower limit of the induced power is about 10% below the reference rotor-induced power.

Figure 9 presents the corresponding induced power factor (namely, the ratio of the power to the ideal theoretical value) vs advance ratio.

The reference rotor and optimized circulation distributions for hover and an advance ratio of 0.2 are shown in Figs. 10–13. In

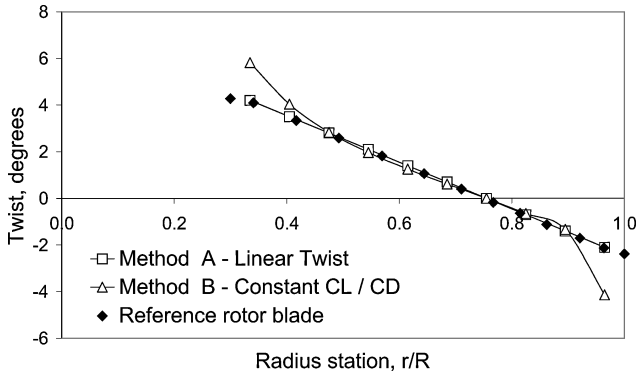

Fig. 7 Blade optimal twist distribution in hover.

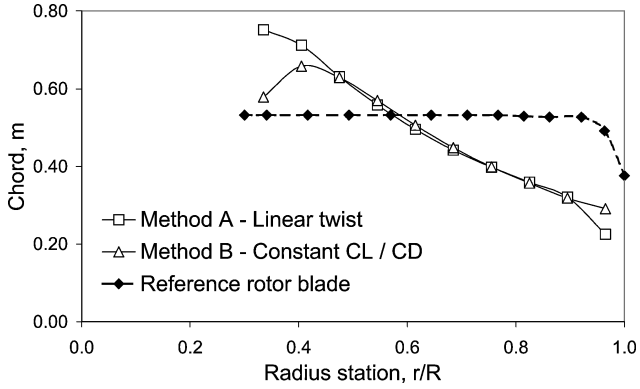

Fig. 8 Blade optimal chord distribution in hover.

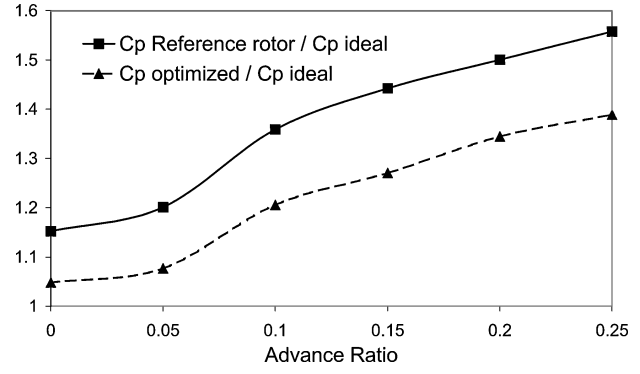

Fig. 9 Induced power factor vs advance ratio.

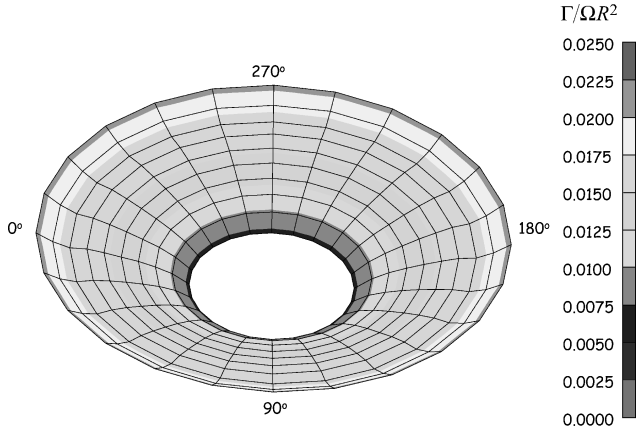

Fig. 10 Circulation distribution for the reference rotor (hover).

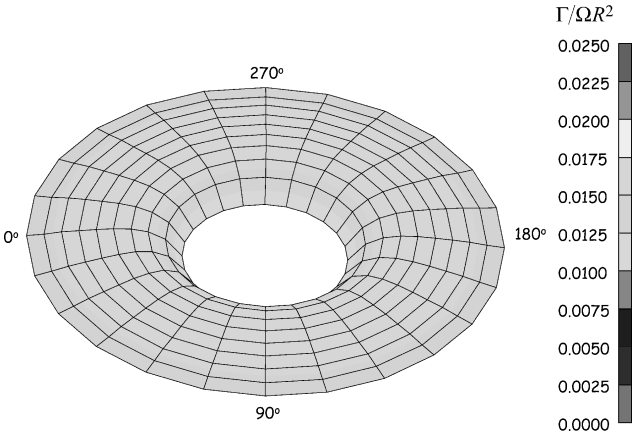

Fig. 11 Circulation distribution for the optimized rotor (hover).

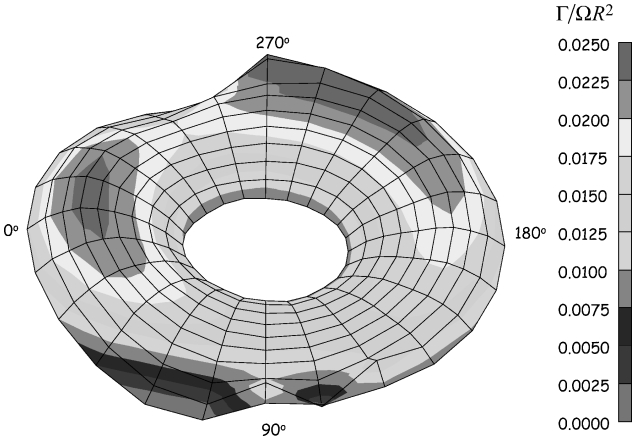

Fig. 12 Circulation distribution for the reference rotor ($\mu = 0.2$).

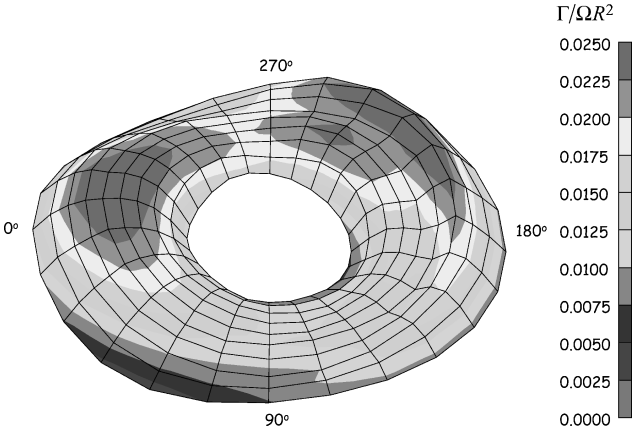

Fig. 13 Circulation distribution for the optimized rotor ($\mu = 0.2$).

hover, the optimized distribution is more uniform. In forward flight the optimized distribution has increased circulation on the forward and aft sides of the rotor disc.

The preceding results can be implemented in hover by conventional design parameters, whereas the implementation in forward flight is much more complicated and can be achieved only by using active devices.

In hover, one can write the distribution of the product of the chord and the lift coefficient as

$$c(r)c_L(r) = \frac{2\Gamma(r)}{\sqrt{[\Omega r]^2 + [v(r)]^2}} \tag{18}$$

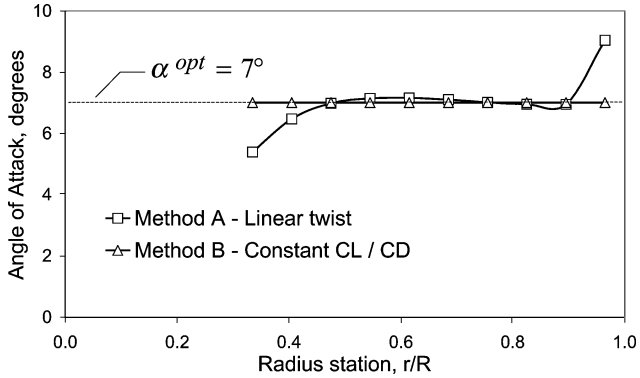

Fig. 14 Blade optimal effective angle-of-attack distribution in hover.

where the right-hand side of the preceding equation is known from the optimization process. At this stage one can apply two ways to proceed. The first way, which will be denoted Method A, assumes linear twist distribution, and, therefore, $c_L(r)$ is given by

$$c_L(r) = c_{L\alpha}\left[\Theta_0 - \Theta_{\text{twist}}\frac{r}{R} - tg^{-1}\left(\frac{v(r)}{\Omega r}\right)\right] \tag{19}$$

Substituting this equation in Eq. (18) yields the chord distribution for this method. In this case Θ_0 and Θ_{twist} can attain any values; however, they should be kept in a certain range that will provide realistic chord and angle-of-attack distributions.

The other way to proceed, which will be denoted Method B, assumes that all cross sections undergo the same optimal effective angle of attack $\alpha^{eff} = \alpha^{opt}$ (i.e., the angle that produces the maximum sectional C_L/C_D value) and therefore produce the same lift coefficient $c_L^{eff} = c_L^{opt}$. Thus, substituting this c_L value in Eq. (18) yields the chord distribution for this method, while the corresponding twist is given by

$$\Theta(r) = \alpha^{opt} + tg^{-1}\left[\frac{v(r)}{\Omega r}\right] \tag{20}$$

Therefore, in Method B both the induced and the sectional drag are minimized.

Figures 7, 8, and 14 present the twist, chord, and the effective angle of attack for the preceding cases.

Conclusions

A method for the determination of the minimum induced power for a helicopter rotor in hover and forward flight is offered. The method is free of the standard design parameters that are usually used for rotor optimization and therefore supplies a generic results for helicopter rotors.

As a generic analysis, this study indicates that compared with a late-1970s reference rotor a reduction of no more then 10% of the induced power can be achieved under any passive or active blade/rotor design (for advance ratios ≤ 0.25).

The limited study of minimum induced power loss by circulation optimization presented in this paper will be expanded in the future. The methodology will be used to explore the following: 1) minimum induced power at high advance ratios including reverse flow regions on the rotor disk; 2) effect of varying number of blades; and 3) effect of trim conditions including propulsive trim (tip-path-plane angle of attack).

References

[1]Johnson, W., *Helicopter Theory*, Dover, New York, 1994.

[2]Prouty, R. W., *Helicopter Performance, Stability, and Control*, Krieger, Malabar, FL, 1990.

[3]Hall, S. R., Yang, K. Y., and Hall, K. C., "Helicopter Rotor Lift Distributions for Minimum-Induced Power Loss," *Journal of Aircraft*, Vol. 31, No. 4, 1994, pp. 837–845.

[4]Moffitt, R. C., and Bissell, J. R., "Theory and Application of Optimum Airloads to Rotors in Hover and Forward Flight," *Proccedings of the 38th Annual Forum of the American Helicopter Society*, Washington, DC, 1982, pp. 1–12.

[5]Quackenbush, T. R., Wachspress, D. A., and Kaufman, A. E., "Optimization of Rotor Performance in Hover Using a Free Wake Analysis," *Journal of Aircraft*, Vol. 28, No. 3, 1991, pp. 200–207.

[6]Nguyen, K., and Chopra, I., "Effects of Higher Harmonic Control on Rotor Performance and Control Loads," *Journal of Aircraft*, Vol. 29, No. 3, 1992, pp. 336–342.

[7]McCloud, J. L., "An Analytical Study of a Multicyclic Controllable Twist Rotor," *Proccedings of the 31st Annual Forum of the American Helicopter Society*, New York, NY, 1975, pp. 932-1–932-10.

[8]Rand, O., "RAPID User Manual," Technion—Israel Inst. of Technology, Haifa, 2000.

[9]Johnson, W., "CAMRAD II, Comprehensive Analytical Model of Rotorcraft Aerodynamics and Dynamics," Volume II: Components Theory Johnson Aeronautics, Palo Alto, CA, 2002, pp. 304–421.

[10]Johnson, W., "A General Free Wake Geometry Calculation for Wings and Rotors," *Proccedings of the 51st Annual Forum of the American Helicopter Society*, Vol. 1, Alexandria, VA, 1995, pp. 137–153.

[11]Johnson, W., "Performance and Loads Data from a Wind Tunnel Test of a Full-Scale Rotor with Four Blade Tip Planforms," NASA TM 81229, Sept. 1980.